ATLAS: ALIBABA DATASET AND BENCHMARK FOR LEARNING-AUGMENTED SCHEDULING

Anonymous authors
Paper under double-blind review

ABSTRACT

Learning-augmented scheduling uses ML predictions to improve decision-making under uncertainty. Many algorithms in this class have been proposed with better theoretical guarantees than the classic methods. Translating these theoretical results into practice, however, requires an understanding of real workloads. Such an understanding is hard to develop because existing production traces either lack the ground-truth processing times or are not publicly available, while synthetic benchmarks fail to represent real-world complexity. We fill this gap by introducing *Alibaba Trace for Learning-Augmented Scheduling (ATLAS)*, a research-ready dataset derived from Alibaba's Platform of Artificial Intelligence (PAI) cluster trace—a production system that processes hundreds of thousands of ML jobs per day. The ATLAS dataset has been cleaned and features engineered to represent the inputs and constraints of non-clairvoyant scheduling, including user tags, resource requests (CPU/GPU/memory), and job structures with ground-truth processing times. We develop a prediction benchmark reporting prediction error metrics, along with feature importance analysis, and introduce a novel multi-stage ML model. We also provide a scheduling benchmark for minimizing the total completion time, max-stretch, and makespan. ATLAS is a reproducible foundation for researchers to study learning-augmented scheduling on real workloads, available at `https://anonymous.4open.science/r/non-clairvoyant-with-predictions-7BF8/`.

1 INTRODUCTION

Modern computing systems have to schedule millions of jobs across without knowing job sizes (i.e., processing time) at submission, a challenge known as non-clairvoyant scheduling. As job sizes are unknown at arrival, the scheduler cannot implement an optimal clairvoyant strategy such as SRPT for total completion time; consequently, non-clairvoyant algorithms achieve suboptimal scheduling performance (Motwani et al., 1994). Learning-augmented algorithms address this performance degradation by incorporating ML job size predictions into online algorithms, improving performance while maintaining worst-case guarantees (Kumar et al., 2018). This framework applies to many domains, and now has grown into an active community (Lindermayr & Megow, 2022).

To illustrate the effect of predictions, consider the single-machine scheduling to minimize total completion time $\sum C_j$, where C_j is the completion time of job J_j, in Figure 1. Suppose we have four jobs released at r_j with unknown sizes p_j^*. Without job predictions, First-In-First-Out (FIFO) runs jobs in arrival order, yielding a total completion time of 51. Round Robin(RR), another good default for non-clairvoyant scheduling (Motwani et al., 1994), achieves $\sum C_j$ of 46.3. With predictions $\hat{p}_j$, Shortest Predicted Job First (SPJF) runs jobs by job size predictions. Even imperfect predictions add value when they roughly reflect relative job order. With true sizes, Shortest Remaining Processing Time (SRPT) is optimal for this problem (Schrage, 1968), yielding a total completion time of 33. Beyond $\sum C_j$, other interesting objectives include maximum stretch, which measures fairness via the maximum ratio of job response time to size $\max_j \frac{C_j - r_j}{p_j^*}$, and makespan $C_{\max} = \max_j C_j$, representing the completion time of the last job, a classic objective in parallel-machine scheduling (Zheng et al., 2023). For each specific objective, recent theoretical work has developed learning-augmented algorithms with provable guarantees (Zhao et al., 2024; Lattanzi et al., 2020; Kumar et al., 2018).

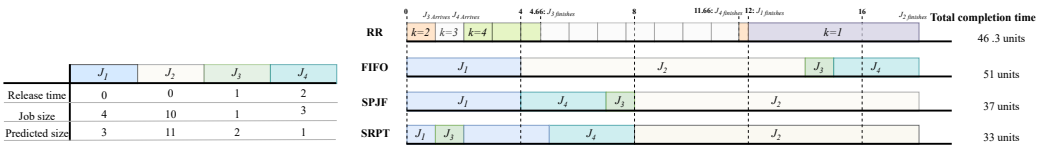

	J_1	J_2	J_3	J_4
Release time	0	0	1	2
Job size	4	10	1	3
Predicted size	3	11	2	1

Figure 1: A toy example showing the comparison of online/offline scheduling algorithms on a single machine with four jobs arriving at $0, 0, 1, 2$ with job sizes $4, 10, 1, 3$ and job size predictions $3, 11, 2, 1$. Despite prediction errors, SPJF, a widely known learning-augmented algorithm, achieves a total completion time of 37, remaining close to SRPT's optimum of 33 and outperforming both Round Robin's 46.3 and FIFO's 51.

However, real production clusters often violate core assumptions underlying these theoretical models. In practice, jobs execute as multi-step workflows (e.g., preprocessing before training) where early-stage failures can terminate the sequence. Furthermore, hardware is heterogeneous and arrivals are stochastic, undermining standard analyses (Weng et al., 2022). These disconnects between theory and practice raise a central question: *How well do learning-augmented schedulers perform in real-world environments?* We address the problem with **Alibaba Trace for Learning-Augmented Scheduling (ATLAS)**, the first dataset for learning-augmented scheduling derived from PAI production clusters, covering over 730,000 jobs with complete execution histories and resource profiles.

Issues with current datasets and benchmarks. First, existing production traces offer limited data for training and evaluating predictors for job processing times. Google's Borg traces (Tirmazi et al., 2020) normalize processing times and obfuscate job identities, removing rich context like user patterns, job types, resource requests, and historical behavior. Azure public datasets (Cortez et al., 2017) and Microsoft's Virtual Machine (VM) allocation traces (Lu et al., 2017) focus primarily on VM provisioning, exposing utilization rates while omitting job structures or exact completion times. The Alibaba trace (Weng et al., 2022) provides job structures but was designed for workload characterization rather than scheduling evaluations. Second, most theoretical studies rely exclusively on synthetic workloads (Zhao et al., 2022; Benomar & Perchet, 2024), limiting job sizes to standard exponential, Pareto, or uniform distributions that miss the complex patterns found in real systems. Third, the field lacks a standardized evaluation benchmark: a clear, reproducible specification of (a) the scheduling framework (online/offline, (non-)preemptive, number of machines), (b) how predictors are trained and validated, and (c) how results are reported and normalized. Consequently, different studies adopt incompatible problem formulations, metrics, and experimental setups, such as work by Fan et al. (2022); Im et al. (2023); Bampis et al. (2023), making cross-paper algorithm comparisons difficult. Furthermore, many overlook temporal constraints (training on past, testing on future), failing to restrict features to historical information, or skip calibration–test separation, risking information leakage that violates non-clairvoyant assumptions (Kapoor & Narayanan, 2023).

1.1 Our work

The ATLAS Dataset. ATLAS transforms raw production traces from Alibaba's Platform of Artificial Intelligence cluster into a dataset designed for scheduling research. The dataset contains completed ML jobs collected from a cluster with over 6,500 GPUs across 1,800 machines. The overview and statistics are shown in Table 1. ATLAS dataset has three defining characteristics:

(1) Non-clairvoyant dataset: Our dataset is non-clairvoyant, where models access only information available at submission time, such as resource plans (resource requests) for CPU, memory, GPU, and instance counts for each task, and identity fields needed to build signatures such as user, group, and workload. We exclude post-execution metrics, actual resource usage, utilization rates, and machine placements, ensuring the ATLAS dataset is research-ready, which replicates a real scheduling environment. *(2) Complete ground-truth job sizes:* Unlike other production traces that omit or normalize runtime information for privacy reasons, ATLAS provides verified processing times for all tasks and jobs. Jobs, with a mean of 1.5 hours, range from 3 seconds to 7 days, with 73.8% completing within one hour and 5.7% exceeding six hours, showing a full spectrum of production workloads. *(3) Rich workload diversity:* ATLAS dataset encompasses jobs with resource requirements spanning from single-CPU tasks to distributed jobs using multiple GPU and GPU clusters, reflecting realistic heterogeneity in CPU/GPU/memory requests. The dataset includes 74.4% single-instance jobs, multi-instance jobs, and distributed jobs with up to 1,050 instances, capturing job scale complexity.

Table 1: ATLAS dataset contains jobs from a two-month Alibaba trace with selected submit-time known and engineered without data-leakage features. ✓ = prediction feature; • = ground-truth label; × = excluded.

Source	Field	Use	Description	Dataset Statistics	
Job	Submission time	✓	Release time r_j; enables temporal patterns	**Dataset splits**	
	User ID	✓	Anonymized submitter (1,314 users)	Training	512,649 (70%)
	Processing time	•	Label $p_j^* = \min_t s_t - \max_t e_t$	Validation	109,853 (15%)
				Test	109,853 (15%)
Task	Task count	✓	Number of roles $[1, 20]$ (median: 1)	**Job size**	
	Planned CPU	✓	$\sum_t n_t r_{t,1}$ $[0, 810\text{K}]$ (median: 6)	Mean	5,382 s (1.5 h)
	Planned GPU	✓	$\sum_t n_t r_{t,2}$ $[0, 40\text{K}]$ (median: 1)	Median	663 s (11 min)
	Planned Memory	✓	$\sum_t n_t r_{t,3}$ $[0.4, 47\text{K}]$ GiB (median: 29)	Std. Dev.	17,095 s
	Instance count	✓	Total parallelism $\sum_t n_t$ $[1, 1050]$	Range	[3 s, 626,384 s]
Group-tag	Group tag	✓	Semantic cluster (65% recurring tasks)	**Job duration**	
	Workload tag	✓	Application type when known	<10 min	355,328 (48.5%)
	GPU spec	✓	Submit-time constraint (V100/P100/T4)	10 min–6 h	335,121 (45.8%)
	Recurrence count	✓	Historical submission frequency	>6 h	41,906 (5.7%)
Engineered	CPU per GPU	✓	Resource ratio $r_{\text{cpu}}/r_{\text{gpu}}$	**Job-scale**	
	Memory per GPU	✓	Resource ratio $r_{\text{mem}}/r_{\text{gpu}}$	Single-instance(1)	544,881 (74.4%)
	Distributed flag	✓	Binary indicator $(n > 1)$	Small (2–10)	93,951 (12.8%)
	User history	✓	Mean/std of user's past submissions	Medium (11–100)	86,380 (11.8%)
	Group history	✓	Mean/std/count of group's past runs	Large (>100)	7,143 (1.0%)
	Scale category	✓	Composite job-scale classification		
Excluded	Assigned GPU	×	Actual placement (V100/P100/T4/Misc)	**GPU categories**	
	Instance IDs	×	Worker/container identifiers	No GPU	17,452 (2.4%)
	Sensor metrics	×	Runtime CPU/GPU/memory utilization	Single GPU	554,179 (75.7%)
	Network usage	×	Bandwidth and I/O measurements	Multi-GPU	110,474 (15.1%)
	Machine specs	×	Hardware configuration details	GPU cluster	50,250 (6.9%)

The LASched Benchmark. Built on top of ATLAS, LASched (Learning-Augmented Scheduling Benchmark) provides a standardized evaluation for the *Prediction Task* on job sizes and *Scheduling Task* of jobs with job size predictions. The prediction benchmark implements multiple baseline models and evaluation metrics, showing that jobs exhibit recurring patterns that can be leveraged for accuracy. LASched enforces leakage-safe construction and restricts features to past-only information available at decision time, preventing future leakage. The scheduling benchmark evaluates classic and learning-augmented schedulers on three metrics—total completion time, maximum stretch, and makespan. With a scheduling benchmark including various baselines, using job size predictions to schedule, the objective values are normalized against the optimum. Together, ATLAS and LASched form a complete platform that enables researchers to develop, evaluate, and compare learning-augmented scheduling methods on real production workloads with reproducible results.

2 The **ATLAS** Dataset

2.1 Data source and formalization

Alibaba PAI–2020 Trace. **ATLAS** is built on the publicly available Alibaba PAI–2020 GPU-cluster trace, which captures two months of MLaaS activity on a large heterogeneous GPU cluster over 6,500 GPUs across ∼1,800 machines (Weng et al., 2022). The trace captures the job life-cycle, including submission, queuing, scheduling, and execution. The trace is relational and organized hierarchically into jobs, tasks, and instances, consistent with established system frameworks such as Google Borg (Verma et al., 2015) and Facebook's Hadoop workloads (Zaharia et al., 2008). Users submit ML jobs through frameworks (e.g., TensorFlow, PyTorch, Graph-Learn); each job is assigned to a scheduler (Fuxi), which translates it into multiple tasks with different roles, e.g., worker, parameter-server (PS), and then instantiates them into Docker containers that are distributed across multiple machines based on resource availability and locality requirements (Weng et al., 2022). Once started, jobs run to completion without preemption. The trace contains only start and end timestamps for each instance, not suspension or resumption events. PAI's monitoring collects per-instance system metrics: CPU/GPU utilization and host/GPU memory, at every 15 seconds via daemon agents that query the Linux kernel and NVIDIA's NVML; the release data also includes machine-level statistics such as network receive throughput. Figure 2 summarizes the job schema, showing hierarchical structure, and the relationship between jobs, planned resources, observed utilization, and machine specifications. We formalize the PAI trace columns so that time semantics,

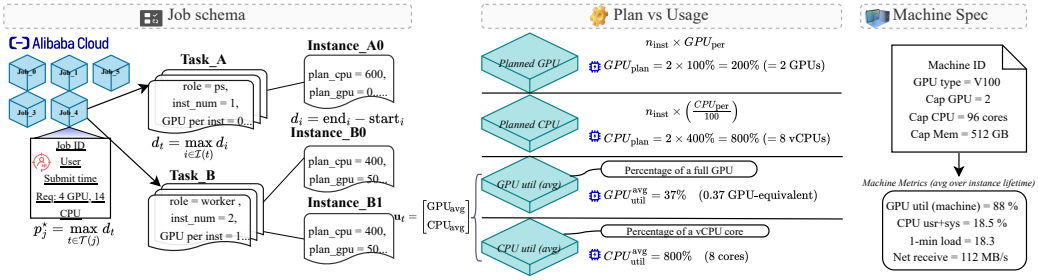

Figure 2: Structure of the Alibaba PAI-2020 GPU cluster trace. Jobs decompose hierarchically into tasks and instances with per-instance resource requirements for GPU and CPU. Job processing time $p_j^* = \max_{t \in \mathcal{T}(j)} d_t$ equals the maximum task duration. The center panel shows planned versus actual resource usage, revealing users requesting more resources than they actually use. Instances can request fractional resources (e.g., 0.5 GPU), supporting resource sharing across multiple jobs. Machine specifications and utilization metrics appear on the right. Task B illustrates gang scheduling $g_t = 1$, where more than one instances start at same time.

label construction, and reproducibility checks are unambiguous, whereas prior analyses of this trace reported workload behavior without a unified mathematical specification.

Job life-cycle: arrivals, queuing, launching. We formalise job life-cycle mathematically as follows. A job J_j arrives at time r_j and consists of tasks $t \in \mathcal{T}(j)$. Each task t declares a per-instance demand vector $\mathbf{r}_t = (r_{t,1}, r_{t,2}, r_{t,3})^\top \in \mathbb{R}^3_+$ representing per-instance GPU, CPU, and memory requests. To be specific, a distributed training worker might request $\mathbf{r}_t = (1, 8, 32)$ for 1 GPU, 8 CPUs, and 32GB memory. Also, each task includes an instance count n_t, and constraints: an admissible GPU-type set Γ_t, a gang flag $g_t \in \{0, 1\}$, and an optional locality flag $\ell_t \in \{0, 1\}$. The cluster comprises machines and each machine m with capacity vector $\mathbf{c}_m = (c_{m,1}, c_{m,2}, c_{m,3})^\top \in \mathbb{R}^3_+$ corresponding to GPU, CPU and memory capacity. While the job waits, the scheduler seeks, for each task t, the earliest time $\tau \geq r_j$ at which its n_t instances admit a feasible placement. Let $\mathcal{I}(t)$ be the instances of t; let $t(i)$ denote the task of instance i; let $x_{i,m}(\tau) \in \{0, 1\}$ indicate that instance i is assigned to machine m at time τ (i.e., $x_{i,m}(\tau) = 1$ if instance i runs on m at time τ, 0 otherwise). Feasibility requires, for every machine m, the resource capacity constraint: $\sum_i x_{i,m}(\tau)\, \mathbf{r}_{t(i)} \leq \mathbf{c}_m$ Where the inequality holds for each resource dimension: GPU, CPU and memory. If $g_t = 1$ then all instances of t must start together, i.e., $\sum_m \sum_{i \in \mathcal{I}(t)} x_{i,m}(\tau) = n_t$; if $\ell_t = 1$ then all instances of t must be co-located on some machine m_t, i.e., $\sum_{i \in \mathcal{I}(t)} x_{i,m_t}(\tau) = n_t$; for GPU-type admissibility, let $g(m)$ denote the GPU type of machine m. We enforce $x_{i,m}(\tau) = 0$, whenever$g(m) \notin \Gamma_t, \forall i \in \mathcal{I}(t)$, $\forall m$, $\forall \tau$, i.e., instances are ineligible for machines of the wrong GPU type. Define the task-ready time $s_t := \inf\{\tau \geq r_j : \text{ a feasible placement for } t \text{ exists at } \tau\}$. The job's start time is the earliest task launch $s_j = \min_{t \in \mathcal{T}(j)} s_t$, and the queuing delay is $q_j = s_j - r_j$. In the PAI trace, the job table's start time stores the submission timer_j, while task and instance tables record the realized launches and finishes. In production, PAI uses reserving-and-packing scheduling: it reserves high-end V100/V100M32 (NVLink) nodes for high-GPU or strict gang/locality tasks, and packs lower-GPU tasks onto T4/older 'Misc' machines via fractional-GPU sharing (Weng et al., 2022).

Job processing time. For every instance i we record its start and end time (s_i, e_i) and the duration as $d_i = e_i - s_i$. For each task t with instances $\mathcal{I}(t)$, define $s_t = \min_{i \in \mathcal{I}(t)} s_i$, $e_t = \max_{i \in \mathcal{I}(t)} e_i$, and $d_t = e_t - s_t$. Let $S = \min_t s_t$ and $E = \max_t e_t$. The job-level processing time is:

$$p_j^* = E - S$$

For any task t, $d_t = e_t - s_t \leq E - S = p_j^*$, hence $\max_t d_t \leq p_j^*$. Prior work by Weng et al. (2022) trains a regressor on instance records and predicts a per-instance duration $\hat{d}_i$; scheduling and error evaluation are performed at the instance granularity. When a value is summarized for a task, it is the mean across that task's instances, $\bar{d}_t = \frac{1}{|\mathcal{I}(t)|} \sum_{i \in \mathcal{I}(t)} d_i$. In contrast, we define the job-level label without using the mean task duration: $\max_t e_t - \min_t s_t$, which matches the classic fork–join completion rule: a task completes when all of its instances complete, and a job completes when all of its tasks complete (Blumofe & Leiserson, 1999; Ko & Serfozo, 2004). Under gang scheduling

Table 2: Three representative job examples from the ATLAS submit-time dataset, and the processing time serves as the prediction label representing the uninterrupted execution duration.

Job Type	pai_job_table				pai_task_table				pai_group_tag_table			Processing Time
	job_name	user_id	submit_time	tasks	instances	cpu (%)	gpu (%)	mem (GB)	group_tag	workload	recurrence	(Label)
Small Inference	d7eb43b8...	5b1345f0...	09:23:15	1	1	600	25	29.3	6c0d75d7...	-	47	**136 s**
Distributed Training	84afa920...	d4d51aca...	10:45:30	2	26	15,100	625	52.0	aba828a1...	**ctr**	12	**9,493 s**
Large Scale	e6145fb3...	df2899e2...	14:12:45	2	105	55,000	4,000	2,050.8	e9d4c564...	-	3	**44,632 s**

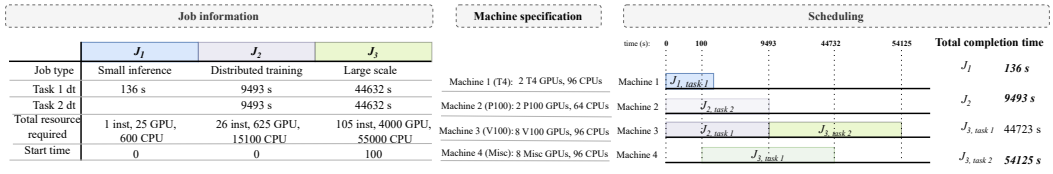

Figure 3: SRPT scheduling of three real PAI jobs. The table shows job characteristics. The timeline illustrates how jobs are allocated: Job 1 (small inference) completes quickly on Machine 1; Job 2 (distributed training) runs tasks in parallel on Machines 2 and 3; Job 3 (large scale) has Task 1 starting immediately on Machine 4 while Task 2 waits for Machine 3, demonstrating the impact of resource heterogeneity on scheduling decisions.

($g_t = 1$), $\sum_m \sum_{i \in \mathcal{I}(t)} x_{i,m}(\tau) = n_t$, instances of a task start together ($s_i = s_t$), so $d_t = \max_i d_i$ and per-instance predictions can be used as task size directly. Weng et al. (2022) report that 85% of task instances in the PAI trace require gang scheduling; in the remaining cases, instances may start at different times, such as one at 0s and one at 50s, but both lasting 100s. The same policies apply to job level. We propose $p_j^\star$ that is reconstructed from timestamps in the task table, not just using the mean task size, which is a more pessimistic method. Admittedly, neither definition decouples the true job demand from Fuxi's historical allocation decisions; allocation preferences and CPU-bound contention remain embedded in the recorded durations. However, the trade-off lies in safety. $\bar{d}_t \leq d_t$ filters skew systematically underestimates occupancy for gang-scheduled tasks where tail determines release. Conversely, $p_j^\star$ captures actual system constraints. We explicitly enforce robustness.

Resource metrics and utilization. Let resource coordinates $k \in \{1, 2, 3\}$ denote GPU, CPU, and memory, respectively. We distinguish submit-time requests from post-execution utilization metrics. Each task t declares a per-instance request $\mathbf{r}_t = (r_{t,1}, r_{t,2}, r_{t,3})$ and instance count n_t, yielding total request $\mathbf{R}_t = n_t \, \mathbf{r}_t$. For job j with tasks $\mathcal{T}(j)$, the submit-time request known at arrival is $\mathbf{R}_j = \sum_{t \in \mathcal{T}(j)} \mathbf{R}_t$. These submit-time quantities $\{\mathbf{r}_t, n_t, \mathbf{R}_j\}$ constitute the prediction features available at scheduling time. Post-execution, instance i runs on interval $[s_i, e_i)$ with duration $d_i = e_i - s_i$ on machine $m(i)$ having capacity vector $\mathbf{c}_{m(i)}$. Let $\tilde{u}_{i,k} \in [0, 1]$ denote the time-averaged utilization fraction of resource k for instance i; the resource–time consumed is $A_{i,k} = \tilde{u}_{i,k} \, c_{m(i),k} \, d_i$. Aggregating to tasks and jobs yields $A_{t,k} = \sum_{i \in \mathcal{I}(t)} A_{i,k}$ and $A_{j,k} = \sum_{t \in \mathcal{T}(j)} A_{t,k}$. Over reporting horizon $H > 0$, the average utilization of machine m on resource k is $\bar{u}_{\text{host},k}(m) = \frac{1}{H \, c_{m,k}} \sum_{i \in \mathcal{I}(m)} A_{i,k}$. With cluster capacity $C_k = \sum_m c_{m,k}$, the cluster-level utilization is $\bar{u}_{\text{cluster},k} = \frac{1}{H \, C_k} \sum_j A_{j,k}$. These realized usage metrics $\{\tilde{u}_{i,k}, A_{\cdot,k}, \bar{u}_{\cdot,k}\}$ are computed after job completion for workload characterization and data validation, not for prediction (Verma et al., 2015; Jeon et al., 2019; Weng et al., 2022).

2.2 Dataset description

Revised data columns. We extract submit-time features from three of the original Alibaba's PAI joint tables to build a dataset for learning-augmented non-clairvoyant scheduling, specified by Table 1. From the *job table*, we keep job's start time and user ID as features, while task and instance timestamps are used solely to compute the ground-truth processing time $p_j^* = \max_t e_t - \min_t s_t$. The *task table* provides resource requirements (CPU, GPU, memory) and parallelism metrics (task and instance counts), aggregated to job level; we exclude assigned GPU types as these reflect post-submission scheduling decisions. The *group-tag table* contributes semantic identifiers and GPU specifications that encode submission-time constraints and recurrence patterns. The remaining tables, sensor and instance, are excluded as they contain either redundant information, post-execution metrics, or scheduling-dependent outcomes incompatible with non-clairvoyant scheduling. Table 5 illustrates data columns with real information for representative jobs derived from the ATLAS.

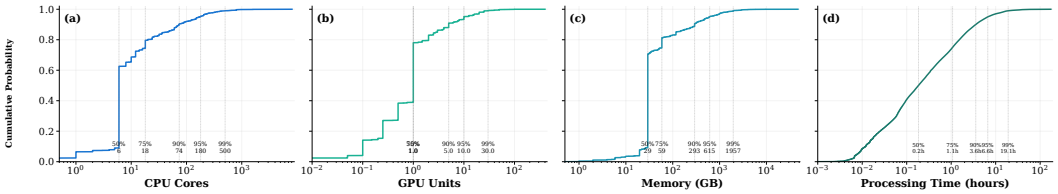

Figure 4: Resource demand and processing-time distributions in the PAI workload. Panels (a)–(c) plot cumulative distribution function (CDF) of per-job requested resources on a log-scaled x-axis with a common y-axis, Cumulative Probability. (a) total requested CPU cores, (b) total requested GPUs, and (c) total requested memory (GiB). Requests are computed as per-instance plans multiplied by instance count and aggregated per job. (d) shows the CDF of per-job p_j^*, defined as the elapsed time from the first task launch to the job's completion.

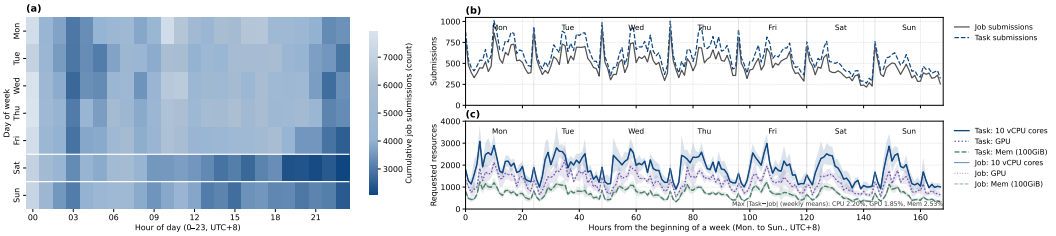

Figure 5: Temporal patterns of submissions and planned resource demand.(a) Heatmap of cumulative job submissions by weekday (rows) and hour (columns). (b) Weekly mean job submissions per hour over complete Monday–Sunday weeks (jobs and tasks).(c) Weekly means of total planned requests from obtained from per-task, per-instance plans $n_t \mathbf{r}_t$ (CPU, GPU, memory); shaded bands show 95% confidence intervals across weeks.

Case study. Figure 3 illustrates heterogeneous-GPU scheduling on representative PAI jobs. For this case study we assume SRPT with known processing times; the goal is to illustrate how trace semantics and resource constraints impact on execution. The small inference job (136 s) is prioritized and finishes quickly, minimizing its impact on throughput. The distributed training job, though longer, exploits parallelism with tasks running concurrently on different nodes. The large-scale job, arriving at t=100, shows how task-level scheduling adds flexibility: Task 2 starts immediately on available machine 4, while Task 1 queues for a V100 due to GPU-type locality. This yields asymmetric task completions (44,732 s vs. 54,125 s), with the job's finish dictated by the slower task.

2.3 Work load characterization

Data cleaning. We keep only *terminated* jobs/tasks and drop rows with missing timestamps or non-positive instance counts. In the trace, timestamps are converted to UTC+8, and for any time–series statistics we restrict to complete Monday–Sunday weeks, discarding partial weeks to avoid edge cases; this dataset choice improves comparability and reduces noise. We reproduced the instance–anchored plot in Weng et al. (2022) for verification, but our scope is on job– and task–level.

Heavy-skewed distribution. The PAI workload exhibits extreme heterogeneity at the job level, with distributions showing severe right-skew. Skewness is 11.02 for processing time and coefficient of variation is larger than 3 for resources. As shown in Figure 4, resource requests size 3–5 orders of magnitude: CPUs (0–8,100 cores), GPUs (0–400 units), and memory (0.4 GB–47 TB). Processing times vary from seconds to days, with the 99th percentile (19.1 hours) being 106× the median: 11 minutes. The workload stratifies into distinct scales: 74% single-instance jobs versus distributed jobs with up to 1,050 instances, and 66% tiny jobs (median 7-minute runtime) versus 1% massive jobs (median 77-minute runtime). This compound heterogeneity—where a small fraction of jobs dominate resource consumption—necessitates log transformation, which reduces skewness from 11.02 to 0.17 and scale-aware modeling for effective learning-augmented scheduling.

Temporal pattern. The trace exhibits strong diurnal/weekly regularity: weekends have fewer submissions, and late–night hours show higher arrivals, consistent with prior production studies (Tirmazi et al., 2020; Reiss et al., 2011). Whereas Weng et al. (2022) visualize a single week, we report the weekly average across complete weeks, shown in Figure 5, which smooths episodic spikes and

yields a more stable signature. Concretely, letting $h \in \{0, \ldots, 167\}$ index hour–of–week and w index weeks, we average hourly request series (e.g., task–anchored $T_w(h)$ and job–anchored $J_w(h)$ formed from planned totals $\mathbf{R}_t = n_t \mathbf{r}_t$) as $\bar{T}(h) = |\mathcal{W}|^{-1} \sum_{w \in \mathcal{W}} T_w(h)$ and analogously for $\bar{J}(h)$. In our data, $\bar{T}(h)$ and $\bar{J}(h)$ are nearly identical, reflecting that most tasks launch within the job's start hour, while the averaged curves remain less sharp, but more robust than a single-week analysis.

3 BENCHMARK

3.1 PREPARATION

Data pre-processing. We use the ATLAS dataset, which constructs a submit-time, job-level table by joining the job, task, and group-tag relations from ALIBABA PAI trace and retaining only terminated records. Timestamps are parsed as seconds, and empty rows are removed. For each task t with instances, we set $s_t = \min_i s_{t,i}, \quad e_t = \max_i e_{t,i}$, and define the job processing time as $p_j^* = \max_t e_t - \min_t s_t$. Jobs with $p_j^\star \leq 0$ are discarded. The submission time r_j anchors chronology and all causal features. Submit-time resource declarations are aggregated per job by summing the times of per-task plans multiplied by their multiplicity, and details are in Table 1. We join the group tag, user identifier, workload tag, and requested GPU specification via the instance identifier; assigned hardware and any post-submission outcomes are excluded. To avoid leakage, we split by r_j: the earliest 70% for training, next 15% for validation, and final 15% for testing. Before training, we run simple checks and use log-transformed $p_j^\star$ as the prediction target to stabilize heavy tails.

Feature engineering. From raw PAI ATLAS data. including 13 columns, we engineer 40 additional features into 53 data frame columns, filtering to 33 model features after removing identifiers and intermediates. All encoders and statistics use training data only. (1) *Resources:* log-transformed totals (CPU, GPU, memory, instances, tasks) and per-instance ratios (CPU/instance, GPU/instance, memory/instance, tasks/instance), addressing the heavy-tailed PAI distributions (Weng et al., 2022) (Figure 4). (2) *Temporal:* sine–cosine hour-of-day encoding to preserve cyclic continuity (Jiang & Zhang, 2009), plus day-of-week and weekend flags. (3) *Recurrence signatures:* concatenate user, group, workload, and decile-bucketed resources; match to historical executions and attach the same train-only statistics such as mean, median, quartiles, standard deviation, and counts. (4) *Historical:* strictly causal, submit-time–ordered expanding statistics for users and groups on $y = \log(1 + p^\star)$—cumulative means, counts, and exponentially weighted moving averages (span=10)—all with one-step lags via `shift(1)`; low-support groups use Empirical Bayes shrinkage ($\lambda = 5$) toward the training-set mean. (5) *Categorical:* user, group, workload, and GPU specification are label-encoded from the training set vocabulary with unseen values mapped to `-1`.

Ablation study and overfitting analysis. The ablation study, using LightGBM, reveals that workload recurrence and group-level execution patterns are the dominant predictive signals (+20.2% over a resource-only baseline), while individual user behaviors provide secondary refinement. The results validate our benchmark design and demonstrate that all using features contribute meaningfully to prediction accuracy, with group-level patterns generalizable across users and resource features transferable across datasets. Our overfitting analysis shows a minimal 1.1% Cov@25% gap between 5-fold cross-validation training and test results, indicating negligible overfitting to the training data. While performance naturally drops for unseen users, a 5.8% gap, due to missing user-specific history, the model maintains robust accuracy by relying on generalizable group and resource features.

3.2 PREDICTION TASK

Prediction models. We model $y_j = \log(1 + p_j^\star)$, where $p_j^\star$ is from earliest task start to latest task end, from submit-time features $\mathbf{x}_j$ using gradient boosting with validation-based calibration. Our methods include, specified in D: (1) *Conformal quantile regression* (CQR) training quantile regressor at α with Ridge-blended final predictions (Romano et al., 2019); (2) *Isotonic calibration* ensuring monotonic probability mapping and adapted for regression/uncertainty calibration (Zadrozny & Elkan, 2002; Kuleshov et al., 2018); (3) *Meta-stacking* combines diverse base models (L2, regularized, quantile, Huber) via gradient boosting on validation predictions (Wolpert, 1992); (4) *Gated*

experts (two-stage): a mixture-of-experts design in which a classifier network routes examples to capacity-matched regressor and aggregates them by soft probabilities (Jordan & Jacobs, 1994); (5) *Weighted recency* uses exponential time-decay $w_t = \exp(-\lambda(T-t))$ for drift adaptation Gama et al. (2014). (6) *Historical Recency-Aware with Shrinkage* uses per-signature means with EB shrinkage to stabilize predictions for rare user-group-resource patterns. All calibrators fit exclusively on validation data following honest prediction principles (Wager & Athey, 2018), with LightGBM (Ke et al., 2017) as our primary regressor using early stopping and monotone constraints if applicable.

Multi-stage predictor. Traditional ML baselines (Classification+Regression and Scale-Bucket Experts) reached only 38–40% Cov@25% in Appendix C, motivating a novel calibration-centric designs. We therefore evaluate methods within one leakage-free framework in Algorithm 1.

Algorithm 1 Multi-Method Job Duration Prediction

Input: time-ordered splits by submit time r_j: D_{train} 70%, $D_{validation}$ 15%, D_{test} 15%
Features: $\mathbf{x}_j = [\mathbf{x}_r, \mathbf{x}_t, \mathbf{x}_h, \mathbf{x}_c]$
  $\mathbf{x}_r$: job totals from task table (CPU/GPU per-inst%$\rightarrow$ counts$\times$inst), log-totals, per-inst ratios
  $\mathbf{x}_t$: $\sin(2\pi h/24)$, $\cos(2\pi h/24)$, day-of-week
  $\mathbf{x}_h$: user/group histories with within-group `shift(1)`; time-since-last-submit
  $\mathbf{x}_c$: categorical (user, group, workload, gpu_type_spec) encoded from D_{tr} only
Target: $y_j = \log(1 + p_j^*)$, where $p_j^* = \max_t e_t - \min_t s_t$ (excludes queuing)
Stage 1 (train on D_{tr}):
  Quantiles: $Q_\alpha \leftarrow$ LGBM (quantile), $\alpha \in \{0.1, 0.5, 0.9\}$
  Regressors: $\{M_k\} \leftarrow$ LGBM with $\{\ell_2, \text{Huber}, \text{regularized}\}$
  Two-Stage: classifier C on tertiles via $\mathcal{Q}_{30,70}(y)$; expert E_c per class
  Recency: R_{full} (time-decay), R_{50}, R_{20} (most recent 50%, 20%)
  Signatures: train-only stats (median/quantiles/count); EB shrinkage $\bar{\mu}_s = \frac{n_s\mu_s + \lambda\mu_0}{n_s+\lambda}$ (λ=5)
Stage 2 (calibrate on D_{va}):
  CQR: on log-target let $r = \max(0, Q_{0.1} - y, y - Q_{0.9})$, $k = \mathcal{Q}_{60}(r)$;
    set bounds $L = Q_{0.1} - k$, $U = Q_{0.9} + k$ (used as features; clip $Q_{0.5}$ to $[L, U]$)
  Blender: $\beta \leftarrow$ Ridge$([L, Q_{0.5}, U, \text{clip}(Q_{0.5}), M_{\ell_2}, \text{priors}])$
  Isotonic: $\phi \leftarrow$ monotone fit of $(Q_{0.5}, y)$ (log domain, clipped)
  Meta: $\psi \leftarrow$ LGBM on $[M_k, \text{dispersion}(M_k), \text{context}]$
  Recency: $\omega_w \propto (\text{MAE}_{\text{va}}(R_w) + \epsilon)^{-1}$; normalize $\sum_w \omega_w = 1$.
Stage 3 (predict on D_{te}):
  CQR: $\hat{y} = \beta([L, Q_{0.5}, U, \text{clip}(Q_{0.5}), M_{\ell_2}, \text{priors}])$; also report $[L, U]$
  Isotonic: $\hat{y} = \phi(Q_{0.5})$; Meta: $\hat{y} = \psi([M_k])$
  Two-Stage: $\hat{y} = \sum_c \pi_c E_c(\mathbf{x})$, with $\pi_c = P(c \mid \mathbf{x})$ from C
  Recency: $\hat{y} = \sum_{w \in \{\text{full},50,20\}} \omega_w R_w(\mathbf{x})$
  HRAS: $\hat{y} = \bar{\mu}_s$; else group EB prior; else global mean
Output: $\hat{p}_j^* = \exp(\hat{y}_j) - 1$ for all methods

3.3 SCHEDULING TASK

Implementation Setup. LASched evaluates objectives under following settings: for **total completion time** ($\sum_j C_j$), a single machine with online arrivals and preemptive scheduling (jobs J_j released at times r_j); for **makespan**, m parallel machines with batch release (all jobs at time 0) and non-preemptive; and for **max-stretch**, a single machine with online arrivals and preemption to capture fairness and prevent starvation of large jobs. Unlike prior work on the original dataset (Weng et al., 2022), which exploits recurring task-level patterns, we study job-level scheduling with imperfect predictions across all job types, scaling from single-machine to thousand-machine clusters.

Baseline Algorithms. For non-clairvoyant baselines, we use FIFO as the online default (Weng et al., 2022), RR, which shares capacity equally among active jobs (Motwani et al., 1994), and LAS (Least-Attained-Service), which prioritizes the job that has received the least service so far (Nuyens & Wierman, 2008). For clairvoyant baselines, which serve as offline performance bounds, we employ SRPT, the optimal for minimizing total completion time (Schrage, 1968), and SJF (Shortest

Job First). For the multi-machine makespan objective, we evaluate LPT (Longest Processing Time), which balances load by assigning the largest job to the least-loaded machine (Della Croce & Scatamacchia, 2020), alongside SPT (Shortest Processing Time) and a Random assignment baseline.

Scheduling Algorithms. These algorithms integrate predictions $\hat{p}_j$ generated by our prediction benchmark models (e.g., CQR, TwoSt) into online decision-making. For **total completion time**, we evaluate SPJF and PRR (Preferential Round-Robin). PRR is a robust mechanism that reserves a processor share λ for the job with the smallest $\hat{p}_j$ while distributing the remaining rate $(1-\lambda)$ equally among all jobs (Kumar et al., 2018). For **max-stretch**, we evaluate SPRPT (SRPT using predicted remaining work) and EDF-P, an Earliest-Deadline-First policy that schedules based on predicted deadlines $d_j = r_j + S_{\text{adv}} \cdot \hat{p}_j$. For **makespan**, we substitute true sizes with predictions to create LPPT (Longest Predicted Processing Time) and SPPT (Shortest Predicted Processing Time), prediction variant of SPT, evaluating how prediction errors impact scheduling policies.

3.4 Evaluation

Prediction error. From theoretical study, $\eta = \max_{1\le j\le n} \max\{\frac{p_j^*}{p_j}, \frac{p_j}{p_j^*}\}$ and $L_1 = \sum_{j=1}^{n} |\hat{p}_j - p_j^*|$ (Kumar et al., 2018; Zhao et al., 2022) are often reported. The community moves toward building a portfolio of metrics rather than a single number (Ahmed et al., 2022), and we propose diverse empirical error metrics for the prediction task. We present Root Mean Squared Logarithmic Error $\text{RMSLE} = \sqrt{\frac{1}{n}\sum_{j=1}^{n}\big(\ln(1+\hat{p}_j) - \ln(1+p_j^\star)\big)^2}$, which de-emphasizes large outliers in heavy-tailed job distributions (Soysal & Streit, 2021). Operational tolerance is captured by Coverage at τ, the fraction of jobs predicted within a relative error τ; we report $\tau \in \{0.25, 0.50\}$: $\text{Cov@}\tau = \frac{100}{n}\sum_{j=1}^{n} \mathbf{1}\Big(\frac{|\hat{p}_j - p_j^\star|}{p_j^\star} \le \tau\Big)$ (Minku & Yao, 2013). Finally, to assess ranking quality, we report Spearman's rank correlation ρ between $\hat{p}_j$ and $p_j^\star$ (Pearson correlation) (Bedő & Ong, 2016).

Scheduling Performance. We evaluate algorithms via empirical competitive ratios against optimal solutions or tight bounds. For **total completion time** $1|r_j, \text{pmtn}|\sum C_j$, we normalize by SRPT: $\rho_{\text{TC}} = \sum_j C_j^{\text{ALG}} / \sum_j C_j^{\text{SRPT}}$. For **makespan** $P||C_{\max}$, we use McNaughton's preemptive bound $\text{OPT}_{\text{pre}} = \max\{\sum_j p_j^*/m, \max_j p_j^*\}$ as baseline: $\rho_{\text{MS}} = C_{\max}^{\text{ALG}}/\text{OPT}_{\text{pre}}$. While non-preemptive makespan is NP-hard, LPT empirically achieves near-optimal performance ($\rho_{\text{MS}} \approx 1$) on our instances. For **max-stretch** $1|r_j, \text{pmtn}|\max_j S_j$, we obtain S^* by bisection on S with EDF-feasibility (Harchol-Balter, 2013), then run EDF at S^* and normalize by the realized $S_{\text{emp}} = \max_j (C_j - r_j)/p_j$, reporting $\rho_{S,\max} = S_{\max}/S_{\text{emp}}$ together with $\rho_{S,99}$ and $\rho_{S,\text{med}}$.

4 Results and Discussion

Table 3 details prediction performance. Two-Stage achieves the best coverage (60.8% Cov@25%, 80.4% Cov@50%) via its classification-first approach, despite similar rank correlations across Two-Stage, Meta-Stack, CQR, and Isotonic. The substantial gap between calibration-centric methods and the history-only HRAS baseline confirms the necessity of job-specific features. Recurring jobs, 81.3% of the test set, exhibit consistently higher accuracy, validating the utility of historical data. Although Meta-Stack offers marginally lower RMSLE, Two-Stage's superior coverage directly yields better scheduling performance. High rank correlation (ρ) explains the outperformance of order-dependent algorithms despite prediction errors. As shown in Table 4, SPJF achieves near-optimal total completion time because the objective prioritizes relative order over accurate prediction size; the 6.8% degradation from SJF to SPJF quantifies the specific cost of prediction error. Furthermore, SPJF outperforms PRR ($\lambda = 0.7$), demonstrating that fully leveraging accurate predicted rankings supersedes partial usage. For makespan, LPPT shows moderate sensitivity, depending primarily on identifying the largest jobs. Preemption mitigates error impact by distributing delays across jobs or m machines, enabling reasonable performance even with HRAS. In contrast, the max-stretch objective is extremely sensitive to prediction quality: a single underestimated large job receives lower priority and accumulates excessive queuing delays, severely degrading the worst-case metric.

Table 3: LASched prediction performance. Cov@25/50 of ground truth. RMSLE and ρ are for *All* only.

Method	Causal History	Val-Only Calib.	Ensemble Type	Cov@25 (%) (All / Rec.)	Cov@50 (%) (All / Rec.)	RMSLE (All)	ρ (All)
CQR-Stack	✓	✓	Conformal	58.3 / 62.9	78.4 / 82.5	0.659	0.950
HRAS	✓	–	None	21.6 / 24.2	40.0 / 43.9	1.455	0.772
QMed+Iso	✓	✓	Single	60.0 / 64.4	79.5 / 83.6	0.689	0.946
LGBM-Meta	✓	✓	Meta-stack	60.0 / 64.4	79.2 / 83.0	**0.656**	0.950
Two-Stage	✓	–	Adaptive	**60.8 / 65.4**	**80.4 / 84.1**	0.658	**0.951**
Weighted-Rec	✓	–	Temporal	52.0 / 55.2	76.5 / 79.8	0.685	0.948

Notes: Recurring = signature seen in training. Splits = 512,647 / 109,854 / 109,854; test recurring = 81.3%

Table 4: Complete scheduling performance across three objectives; lower is better.

(A) Max-Stretch				(B) Total Completion Time		(C) Makespan	
Algorithm	$\rho_{S,\max}$	$\rho_{S,99}$	$\rho_{S,\text{med}}$	**Algorithm**	**Ratio**	**Algorithm**	**Ratio**
OPT (EDF at S^*)	**1.000**	**1.000**	**1.000**	SRPT	**1.000**	LPT	**1.000**
SRPT	1.189	1.150	0.900	SJF	1.001	SPT	1.539
LAS/FB	1005.85	607.79	155.62	RR	1.975	Greedy	1.452
				FIFO	5.372	Random	1.955
CQR-SPRPT	15.69	3.88	0.121	CQR-SPJF	1.075	CQR-LPPT	1.517
CQR-EDF(pred)	4287.21	1214.92	14.65	CQR-PRR	1.252	CQR-SPPT	1.694
HRAS-SPRPT	39.80	24.59	0.235	HRAS-SPJF	1.823	HRAS-LPPT	1.874
HRAS-EDF(pred)	5036.06	1474.90	20.01	HRAS-PRR	1.929	HRAS-SPPT	1.801
Iso-SPRPT	15.58	3.62	0.127	Iso-SPJF	1.087	Iso-LPPT	1.500
Iso-EDF(pred)	4437.21	1233.32	14.99	Iso-PRR	1.265	Iso-SPPT	1.615
Meta-SPRPT	**14.97**	**3.35**	0.125	Meta-SPJF	1.072	Meta-LPPT	1.529
Meta-EDF(pred)	4342.12	1232.13	14.83	Meta-PRR	1.252	Meta-SPPT	1.692
TwoSt-SPRPT	15.63	3.64	**0.119**	TwoSt-SPJF	**1.066**	TwoSt-LPPT	**1.498**
TwoSt-EDF(pred)	4346.84	1212.56	14.68	TwoSt-PRR	1.246	TwoSt-SPPT	1.604
Rec-SPRPT	17.64	3.78	0.120	Rec-SPJF	1.097	Rec-LPPT	1.568
Rec-EDF(pred)	4567.88	1292.03	16.34	Rec-PRR	1.278	Rec-SPPT	1.769

5 Conclusion

We release **ATLAS**, a research-ready dataset with actual job sizes and features over 730k+ cluster jobs for learning-augmented scheduling, and **LASched**, a standardized benchmark for job size prediction and scheduling tasks with an implementation guide. We provide prediction baselines with error evaluation using coverage, RMSLE, and rank correlation. Popular learning-augmented algorithms are implemented with their performance reported. The dataset and baselines are intended to serve as community reference points, demonstrating that LAShed achieves near-optimal performance for common objectives: total completion time and makespan. However, while standard predictors suffice for these aggregate metrics, they fail on tail-sensitive objectives. Exposing these gaps identifies three future directions: (1) asymmetric loss functions to address prediction-scheduling mismatches, (2) distributionally robust optimization (e.g., CVaR) to minimize worst-case stretch, and (3) rank-aware feature learning to prioritize relative ordering. Future work will extend the benchmark with cross-dataset validation and test algorithms on different optimization objectives.

Reproducibility Statement. We make our work reproducible along three aspects: data, prediction, and scheduling. The clear step-by-step user guide, including data downloading notes for different systems, code scripts running suggestions, and a detailed evaluation method, is in anonymized link, referred to readme.md file in the following link: `https://anonymous.4open.science/r/non-clairvoyant-with-predictions-7BF8/`. Three reproducible information are listed.

(i) *Data.* ATLAS is derived from the public Alibaba PAI–2020 trace with a novel formalized job schema and label construction; we release an anonymized repository, shown in abstract, with scripts to rebuild the submit-time job table and ground-truth labels from raw datasets, including checks for terminated rows only and exact time semantics (earliest task start, latest task end). Please see dataset

link in the abstract and Section 2: Dataset. Users can employ this dataset to construct interested columns, such as maximum task duration and instance duration. Also, users can make Python plots to see job size distribution, actual resource utilization rate, which could be both at submit-time or post-execution, any workload characterization preferred.

(ii) *Prediction.* We release code to reproduce the split (70%/15%/15% by submit time), train-only feature engineering (resources, temporal signals, recurrence signatures, strictly causal group/user histories with `shift(1)`, and label encoding), and all six calibrated baselines with validation-only calibration; configuration files and fixed random seeds are provided to regenerate Table 3 end-to-end (Cov@25/50, RMSLE, and Spearman's ρ). Users can use traditional ML models to make job size and task size predictions, which is also provided, and technical details are shown in Appendix C.

(iii) *Scheduling.* The benchmark includes an executable simulator with reference implementations of all policies and the exact normalizations used in Table 4: $\sum_j C_j$ reported relative to SRPT; makespan reported relative to the preemptive lower bound $\mathrm{OPT}_{\mathrm{pre}}$; and max-stretch computed via an EDF-feasibility test at the bisection optimum. Scripts are provided to recreate every number from a fixed commit. In line with the ICLR 2026 Author Guide, we place this statement before the references and supply anonymous code and supplementary materials with the submission; while reviewers are not required to read appendices, the released anonymized repository can reproduce all main tables and figures.

REFERENCES

Nasim Ahmed, Andre LC Barczak, Mohammad A Rashid, and Teo Susnjak. Runtime prediction of big data jobs: performance comparison of machine learning algorithms and analytical models. *Journal of Big Data*, 9(1):67, 2022.

Evripidis Bampis, Alexander Kononov, Giorgio Lucarelli, and Fanny Pascual. Non-clairvoyant makespan minimization scheduling with predictions. In *34th International Symposium on Algorithms and Computation (ISAAC 2023)*, pp. 9–1. Schloss Dagstuhl–Leibniz-Zentrum für Informatik, 2023.

Justin Bedő and Cheng Soon Ong. Multivariate spearman's ρ for aggregating ranks using copulas. *Journal of Machine Learning Research*, 17(201):1–30, 2016.

Ziyad Benomar and Vianney Perchet. Non-clairvoyant scheduling with partial predictions. *arXiv preprint arXiv:2405.01013*, 2024.

Robert D Blumofe and Charles E Leiserson. Scheduling multithreaded computations by work stealing. *Journal of the ACM (JACM)*, 46(5):720–748, 1999.

Eli Cortez, Anand Bonde, Alexandre Muzio, Mark Russinovich, Marcus Fontoura, and Ricardo Bianchini. Resource central: Understanding and predicting workloads for improved resource management in large cloud platforms. In *Proceedings of the 26th Symposium on Operating Systems Principles*, pp. 153–167, 2017.

Federico Della Croce and Rosario Scatamacchia. The longest processing time rule for identical parallel machines revisited. *Journal of Scheduling*, 23(2):163–176, 2020.

Yuping Fan, Zhiling Lan, Paul Rich, William Allcock, and Michael E Papka. Hybrid workload scheduling on hpc systems. In *2022 IEEE International Parallel and Distributed Processing Symposium (IPDPS)*, pp. 470–480. IEEE, 2022.

João Gama, Indrė Žliobaitė, Albert Bifet, Mykola Pechenizkiy, and Abdelhamid Bouchachia. A survey on concept drift adaptation. *ACM computing surveys (CSUR)*, 46(4):1–37, 2014.

Mor Harchol-Balter. *Performance modeling and design of computer systems: queueing theory in action*. Cambridge University Press, 2013.

Sungjin Im, Ravi Kumar, Mahshid Montazer Qaem, and Manish Purohit. Non-clairvoyant scheduling with predictions. *ACM Transactions on Parallel Computing*, 10(4):1–26, 2023.

Myeongjae Jeon, Shivaram Venkataraman, Amar Phanishayee, Junjie Qian, Wencong Xiao, and Fan Yang. Analysis of {Large-Scale}{Multi-Tenant}{GPU} clusters for {DNN} training workloads. In *2019 USENIX Annual Technical Conference (USENIX ATC 19)*, pp. 947–960, 2019.

Wenhua Jiang and Cun-Hui Zhang. General maximum likelihood empirical bayes estimation of normal means. *Journal of the American Statistical Association*, 2009.

Michael I Jordan and Robert A Jacobs. Hierarchical mixtures of experts and the em algorithm. *Neural computation*, 6(2):181–214, 1994.

Sayash Kapoor and Arvind Narayanan. Leakage and the reproducibility crisis in machine-learning-based science. *Patterns*, 4(9), 2023.

Guolin Ke, Qi Meng, Thomas Finley, Taifeng Wang, Wei Chen, Weidong Ma, Qiwei Ye, and Tie-Yan Liu. Lightgbm: A highly efficient gradient boosting decision tree. *Advances in neural information processing systems*, 30, 2017.

Sung-Seok Ko and Richard F Serfozo. Response times in m/m/s fork-join networks. *Advances in Applied Probability*, 36(3):854–871, 2004.

Volodymyr Kuleshov, Nathan Fenner, and Stefano Ermon. Accurate uncertainties for deep learning using calibrated regression. In *International conference on machine learning*, pp. 2796–2804. PMLR, 2018.

Ravi Kumar, Manish Purohit, and Zoya Svitkina. Improving online algorithms via ml predictions. In *Proceedings of the 32nd International Conference on Neural Information Processing Systems*, pp. 9684–9693, 2018.

Silvio Lattanzi, Thomas Lavastida, Benjamin Moseley, and Sergei Vassilvitskii. Online scheduling via learned weights. In *Proceedings of the Fourteenth Annual ACM-SIAM Symposium on Discrete Algorithms*, pp. 1859–1877. SIAM, 2020.

Alexander Lindermayr and Nicole Megow. Algorithms with predictions. `https://algorithms-with-predictions.github.io/`, 2022. Accessed: 2024-01-24.

Chengzhi Lu, Kejiang Ye, Guoyao Xu, Cheng-Zhong Xu, and Tongxin Bai. Imbalance in the cloud: An analysis on alibaba cluster trace. In *2017 IEEE International Conference on Big Data (Big Data)*, pp. 2884–2892. IEEE, 2017.

Leandro L Minku and Xin Yao. Software effort estimation as a multiobjective learning problem. *ACM Transactions on Software Engineering and Methodology (TOSEM)*, 22(4):1–32, 2013.

Rajeev Motwani, Steven Phillips, and Eric Torng. Nonclairvoyant scheduling. *Theoretical computer science*, 130(1):17–47, 1994.

Misja Nuyens and Adam Wierman. The foreground–background queue: a survey. *Performance evaluation*, 65(3-4):286–307, 2008.

Fabian Pedregosa, Gaël Varoquaux, Alexandre Gramfort, Vincent Michel, Bertrand Thirion, Olivier Grisel, Mathieu Blondel, Peter Prettenhofer, Ron Weiss, Vincent Dubourg, et al. Scikit-learn: Machine learning in python. *the Journal of machine Learning research*, 12:2825–2830, 2011.

Charles Reiss, John Wilkes, and Joseph L Hellerstein. Google cluster-usage traces: format+ schema. *Google Inc., White Paper*, 1:1–14, 2011.

Yaniv Romano, Evan Patterson, and Emmanuel Candes. Conformalized quantile regression. *Advances in neural information processing systems*, 32, 2019.

Linus Schrage. A proof of the optimality of the shortest remaining processing time discipline. *Operations Research*, 16(3):687–690, 1968.

Mehmet Soysal and Achim Streit. Collection of job scheduling prediction methods. In *Job Scheduling Strategies for Parallel Processing: 24th International Workshop, JSSPP 2021, Virtual Event, May 21, 2021, Revised Selected Papers 24*, pp. 35–42. Springer, 2021.

Muhammad Tirmazi, Adam Barker, Nan Deng, Md E Haque, Zhijing Gene Qin, Steven Hand, Mor Harchol-Balter, and John Wilkes. Borg: the next generation. In *Proceedings of the fifteenth European conference on computer systems*, pp. 1–14, 2020.

Abhishek Verma, Luis Pedrosa, Madhukar Korupolu, David Oppenheimer, Eric Tune, and John Wilkes. Large-scale cluster management at google with borg. In *Proceedings of the tenth european conference on computer systems*, pp. 1–17, 2015.

Stefan Wager and Susan Athey. Estimation and inference of heterogeneous treatment effects using random forests. *Journal of the American Statistical Association*, 113(523):1228–1242, 2018.

Qizhen Weng, Wencong Xiao, Yinghao Yu, Wei Wang, Cheng Wang, Jian He, Yong Li, Liping Zhang, Wei Lin, and Yu Ding. {MLaaS} in the wild: Workload analysis and scheduling in {Large-Scale} heterogeneous {GPU} clusters. In *19th USENIX Symposium on Networked Systems Design and Implementation (NSDI 22)*, pp. 945–960, 2022.

David H Wolpert. Stacked generalization. *Neural networks*, 5(2):241–259, 1992.

Bianca Zadrozny and Charles Elkan. Transforming classifier scores into accurate multiclass probability estimates. In *Proceedings of the eighth ACM SIGKDD international conference on Knowledge discovery and data mining*, pp. 694–699, 2002.

Matei Zaharia, Andy Konwinski, Anthony D Joseph, Randy H Katz, and Ion Stoica. Improving mapreduce performance in heterogeneous environments. In *Osdi*, volume 8, pp. 7, 2008.

Tianming Zhao, Wei Li, and Albert Y Zomaya. Uniform machine scheduling with predictions. In *Proceedings of the International Conference on Automated Planning and Scheduling*, volume 32, pp. 413–422, 2022.

Tianming Zhao, Xiaomin Chang, Chunhao Li, Wei Li, Albert Zomaya, et al. Competitive fair scheduling with predictions. In *The Thirteenth International Conference on Learning Representations*, 2024.

Pengfei Zheng, Rui Pan, Tarannum Khan, Shivaram Venkataraman, and Aditya Akella. Shockwave: Fair and efficient cluster scheduling for dynamic adaptation in machine learning. In *20th USENIX Symposium on Networked Systems Design and Implementation (NSDI 23)*, pp. 703–723, 2023.

A NOTATIONS

A.1 BASIC ENTITIES AND TIME VARIABLES

Symbol	Name	Meaning	Example
J_j	Job	A job submitted by a user	Training job for classifier
t	Task	A role within a job	Worker task in distributed training
i	Instance	One copy of a task running	Worker instance #3 out of 10
m	Machine	Physical server in cluster	Server with 8 V100 GPUs
r_j	Arrival time	When job was submitted	Submitted at 10:00 AM
τ	Time variable	Any point in time	Checking availability at 10:15 AM
s_t	Task start time	When task begins running	Task starts at 10:30 AM
s_j	Job start time	When first task starts	Job starts with earliest task
q_j	Queuing delay	Time spent waiting	Waited 30 minutes for resources

A.2 SETS AND COLLECTIONS

Symbol	Name	Meaning	Example
$T(j)$	Task set	All tasks belonging to job j	{PS, Worker, Evaluator}
$I(t)$	Instance set	All instances of task t	{Worker-1, ..., Worker-10}
Γ_t	GPU type set	Compatible GPU types	{V100, P100} but not T4

A.3 RESOURCE VECTORS AND DEMANDS

Symbol	Name	Meaning	Example
$\mathbf{r}_t$	Resource request	Resources per instance	[2 GPUs, 16 CPUs, 64GB RAM]
$\mathbf{c}_m$	Machine capacity	Total machine resources	[8 GPUs, 96 CPUs, 512GB RAM]
n_t	Instance count	Number of task copies	10 worker instances

A.4 RESOURCE UTILIZATION

A.5 JOB PROCESSING TIME CALCULATION

We define job processing time based on a hierarchical Fork-Join model.

1. Instance Duration For an instance i running on the interval $[s_i, e_i)$:

$$d_i = e_i - s_i \tag{1}$$

2. Task Span (Fork-Join for Instances) A task t completes only when its last instance finishes.

$$s_t = \min_{i \in I(t)} s_i, \quad e_t = \max_{i \in I(t)} e_i \tag{2}$$

$$d_t = e_t - s_t = \max_{i \in I(t)} e_i - \min_{i \in I(t)} s_i \tag{3}$$

Note: For gang-scheduled tasks ($g_t = 1$), $s_i = s_t$ for all i, so $d_t = \max_i d_i$.

3. Job Processing Time (Fork-Join for Tasks) A job J_j completes only when its last task finishes.

$$S = \min_{t \in T(j)} s_t, \quad E = \max_{t \in T(j)} e_t \tag{4}$$

$$p_j^* = E - S \tag{5}$$

This definition correctly captures the true resource occupancy window, including barriers from staggered task starts, unlike mean-based aggregations.

Symbol	Name	Meaning	Example
$\mathbf{R}_t$	Total task request	$\mathbf{R}_t = n_t \cdot \mathbf{r}_t$	Total resources for all workers
$\mathbf{R}_j$	Total job request	$\mathbf{R}_j = \sum_{t \in T(j)} \mathbf{R}_t$	Sum of all tasks' requests
$u_{i,k}$	Instance utilization	Average usage of resource k by instance i	85% GPU usage over execution
$A_{i,k}$	Resource-time	$A_{i,k} = u_{i,k} \cdot c_{m(i),k} \cdot d_i$	Total GPU-seconds consumed

A.6 Key Scheduling Constraints

1. Resource Capacity Constraint

$$\sum_i x_{i,m}(\tau) \cdot \mathbf{r}_{t(i)} \leq \mathbf{c}_m \tag{6}$$

Total resources used by all instances on a machine cannot exceed that machine's capacity

2. Gang Scheduling Constraint (when $g_t = 1$)

$$\sum_m \sum_{i \in I(t)} x_{i,m}(\tau) = n_t \tag{7}$$

All n_t instances of the task must be placed at the same time τ

3. Locality Constraint (when $\ell_t = 1$)

$$\sum_{i \in I(t)} x_{i,m_t}(\tau) = n_t \tag{8}$$

All instances must be on the same machine m_t

4. GPU Type Constraint

$$x_{i,m}(\tau) = 0 \quad \text{when } g(m) \notin \Gamma_t \tag{9}$$

Cannot place instances on machines with incompatible GPU types

B Dataset Characteristics and Job Examples

To illustrate the diversity of workloads in the ATLAS dataset and clarify the nature of the Processing Time label, Table 5 presents three representative jobs drawn directly from the trace. These examples showcase different scales of operation, from small inference tasks to large-scale distributed training.

Crucially, the workloads captured in the Alibaba PAI trace are non-preemptible. Once a job begins execution, it runs to completion without interruption by the scheduler. Therefore, the Processing Time reported in the final column of Table 5 represents the actual, continuous duration of the job from start to finish. This single value accurately reflects the job's size for prediction tasks, as there are no preemption or resumption dynamics to model. The table highlights key features used for prediction, such as the number of tasks and instances, requested resources (CPU, GPU, memory), and workload type. The wide range of processing times, from just over two minutes to more than 12 hours, demonstrates the challenge of the prediction task.

Table 5: Three representative job examples from the ATLAS submit-time dataset, illustrating different job types, scales, and their corresponding processing times. The Processing Time serves as the prediction label and represents the uninterrupted execution duration, as jobs in this trace are not preempted.

Job Type	pai_job_table				pai_task_table				pai_group_tag_table			Processing Time
	job_name	user_id	submit_time	tasks	instances	cpu (%)	gpu (%)	mem (GB)	group_tag	workload	recurrence	(Label)
Small Inference	d7eb43b8...	5b1345f0...	09:23:15	1	1	600	25	29.3	6c0d75d7...	-	47	**136 s**
Distributed Training	84afa920...	d4d51aca...	10:45:30	2	26	15,100	625	52.0	aba828a1...	ctr	12	**9,493 s**
Large Scale	e6145fb3...	df2899e2...	14:12:45	2	105	55,000	4,000	2,050.8	e9d4c564...	-	3	**44,632 s**

C TRADITIONAL ML PREDICTION MODELS TRIED

Our preliminary methods explored four baselines: (1) a single-stage gradient-boosted trees model on the log target with monotone constraints on obvious scale features (instances, GPUs), to encode weak priors and reduce pathological splits in sparse regions Ke et al. (2017). (2) a CRR++ "cluster→route→refit" variant that forms train-only k-means families, learns a router, and applies per-family experts with a global fallback—useful when coarse workload types exist but are unlabeled Pedregosa et al. (2011). (3) scale-bucket experts using train-quantile edges on instance/GPU counts to fit per-bucket regressor, again with a global fallback; and (4) a simple recency ensemble mixing a full-history model with a recent-window model to hedge concept drift Gama et al. (2014). These baselines improved over naive single models but exposed core gaps: poor uncertainty calibration and tail handling (heavy-tailed durations), weak rank fidelity in some regimes, brittle behavior for signatures, and limited drift adaptation from fixed mixtures. So, bad performances motivated our current seven-method toolkit that adds calibrated quantile intervals and blending, explicit monotone-safe calibration (isotonic), diversity via stacking, a principled gated-experts split, stronger recency weighting with validation-based ensembling, and empirical-Bayes priors for sparse signatures—addressing calibration, ranking, sparsity, and drift more systematically than the four preliminaries could alone.

Algorithm 2 Common preprocessing (used by M1–M4)

1: **Input:** raw tables (job, task, tag), submit time r_j, label $p_j^\star$, features $\mathbf{x}_j$
2: **Split by time:** sort by r_j; pick cut times $t_{\text{train}} < t_{\text{val}}$; define $\mathcal{D}_{tr} = \{j : r_j < t_{\text{train}}\}$, $\mathcal{D}_{va} = \{j : t_{\text{train}} \le r_j < t_{\text{val}}\}$, $\mathcal{D}_{te} = \{j : r_j \ge t_{\text{val}}\}$.
3: **Core features (submit-time only):** logs of totals ($\log(1+x)$ for CPU/GPU/MEM/instances/tasks), per-instance ratios, cyclic time (`hour`, `wday`, sin / cos of 24h and 168h).
4: **Causal histories (group/user):** on the *log target* $y_j = \log(1 + p_j^\star)$, compute within-group expanding means and counts with a one-step `shift(1)`; time since previous submit; small shifted rolling means; an empirical-Bayes (EB) group mean μ^{EB} using only $\mathcal{D}_{tr}$ to set the global prior μ_0.
5: **Train-only encodings:** map `user`/`group`/`workload`/`gpu_type_spec` to integer codes using the vocabulary in $\mathcal{D}_{tr}$; unseen $\mapsto$ `OTHER`.
6: **Sanity:** replace $\pm\infty$ and NaNs with 0 for numeric features; **never** touch labels in $\mathcal{D}_{va}, \mathcal{D}_{te}$ beyond metrics.
7: **Return:** design matrices X_{tr}, X_{va}, X_{te} and vectors $y_{tr} = \log(1 + p^\star)$, y_{va}, $y_{te} = p^\star$.

Algorithm 3 M1 — Single-Stage Gradient Boosting (log target) with causal histories

1: **Input:** X_{tr}, X_{va}, X_{te} from Alg. 2; y_{tr}, y_{va}, y_{te}
2: **(optional) Monotone constraints:** choose a feature subset $\mathcal{M}^+$ expected to be non-decreasing (e.g., $\log(1 + \text{instances})$, $\log(1 + \text{GPU})$) and pass a monotonicity vector to the booster.
3: Train a gradient-boosted trees regressor on y_{tr} with early stopping on (X_{va}, y_{va}) (all log-domain).
4: **Predict:** $\hat{y}_{te} \leftarrow \text{model}(X_{te})$; return $\hat{p}_{te} = \exp(\hat{y}_{te}) - 1$.
5: **Metrics:** report Cov@25/50, RMSLE, MAE, and Spearman on $(\hat{p}_{te}, y_{te})$.

Algorithm 4 M2 — CRR++ (Cluster → Route → Refit) with per-family experts

1: **Input:** X_{tr}, X_{va}, X_{te}; y_{tr}, y_{va}, y_{te}; clusters K; min-support $n_{\min}$
2: **Standardize (train-only):** fit a scaler on X_{tr}; transform to Z_{tr}, Z_{va}, Z_{te}.
3: **Unsupervised families (train-only):** fit K-means on Z_{tr}; obtain family IDs f_{tr}; assign f_{va}, f_{te} by `predict`.
4: **Router (train-only):** train a multi-class classifier to map $Z \mapsto f$ using (Z_{tr}, f_{tr}).
5: **Fallback regressor:** train a global log-target booster on (X_{tr}, y_{tr}) with early stopping on (X_{va}, y_{va}).
6: **Per-family experts:** for each $k \in \{1, \ldots, K\}$ with $\#\{j \in \mathcal{D}_{tr} : f_{tr}(j) = k\} \ge n_{\min}$, train a log-target booster on the subset $\{j : f_{tr}(j) = k\}$; optionally use $(X_{va}[f_{va} = k], y_{va}[f_{va} = k])$ for early stopping.
7: **Predict:** for each test sample x, set $\hat{k} \leftarrow \text{router}(z)$; if expert $k = \hat{k}$ exists use it, else use the fallback; return $\hat{p} = \exp(\hat{y}) - 1$.
8: **Metrics:** as in Alg. 3.

Algorithm 5 M3 — Scale-Bucket Experts (train-quantiles → per-bucket models)

1: **Input:** X_{tr}, X_{va}, X_{te}; y_{tr}, y_{va}, y_{te}; train-only features a = instances, b = GPU; min-bucket $n_{\min}$
2: **Train-only bucket edges:** compute quantiles Q_a and Q_b on (a, b) over $\mathcal{D}_{tr}$ (e.g., $\{0.5, 0.9, 0.99\}$); define bucketizers $\text{bin}_a, \text{bin}_b$.
3: **Assign buckets:** $u_j = \max\{\text{bin}_a(a_j), \text{bin}_b(b_j)\}$ for all j in train/val/test.
4: **Global fallback:** train a log-target booster on all of $\mathcal{D}_{tr}$ with early stopping on $\mathcal{D}_{va}$.
5: **Per-bucket experts:** for each bucket u with $\#\{j \in \mathcal{D}_{tr} : u_j = u\} \geq n_{\min}$, train a log-target booster on $\{j : u_j = u\}$; optionally early-stop on $\{j \in \mathcal{D}_{va} : u_j = u\}$.
6: **Predict:** for each test sample with bucket u, use expert(u) if available; else use the global fallback; return $\hat{p} = \exp(\hat{y}) - 1$.
7: **Metrics:** as in Alg. 3.

Algorithm 6 M4 — Recency Ensemble (full vs. recent window; train-only gates)

1: **Input:** X_{tr}, X_{va}, X_{te}; y_{tr}, y_{va}, y_{te}; training times $\{r_j : j \in \mathcal{D}_{tr}\}$; window quantile q; mixture weight α
2: **Full model:** train a log-target booster on (X_{tr}, y_{tr}); early-stop on (X_{va}, y_{va}).
3: **Recent cut (train-only):** set $t_q \leftarrow \text{Quantile}_q(\{r_j : j \in \mathcal{D}_{tr}\})$; define $\mathcal{D}_{tr}^{\text{recent}} = \{j \in \mathcal{D}_{tr} : r_j \geq t_q\}$.
4: **Recent model (if enough support):** train a log-target booster on $\mathcal{D}_{tr}^{\text{recent}}$, early-stopped on (X_{va}, y_{va}); otherwise skip.
5: **Predict & mix:** let $\tilde{p}^{(full)} = \exp(\hat{y}^{(full)}) - 1$, $\tilde{p}^{(rec)} = \exp(\hat{y}^{(rec)}) - 1$ (if present); output $\hat{p} = (1-\alpha)\tilde{p}^{(full)} + \alpha\,\tilde{p}^{(rec)}$ if recent model exists, else $\tilde{p}^{(full)}$.
6: **Metrics:** as in Alg. 3.

Results. The corresponding prediction metrics are summarized below in Table 6.

Table 6: Preliminary prediction methods (leakage-safe). Cov@25/50 reported as *All / Rec.*; RMSLE and ρ are for *All*.

Method	Causal History	Val-Only Calib.	Ensemble Type	Cov@25 (%) (All / Rec.)	Cov@50 (%) (All / Rec.)	RMSLE (All)	ρ (All)
M1 Single-Stage (LGBM, log-target)	✓	–	Single	39.9 / —	61.3 / —	1.002	0.885
M2 CRR++ (KMeans+router+experts)	✓	–	Cluster-experts	40.0 / —	61.8 / —	1.016	0.882
M3 Scale-Bucket Experts	✓	–	Scale-experts	39.0 / —	59.8 / —	1.072	0.867
M4 Recency Ensemble (full+recent)	✓	–	Temporal	38.4 / —	59.7 / —	1.040	0.878

Notes: "Rec." values are unavailable for these preliminary runs; dashes indicate not reported. All methods use leakage-safe, time-ordered splits with submit-time features only.

D PREDICTION MODEL DESCRIPTION

We model $y_j = \log(1 + p_j^\star)$ from submit-time features $\mathbf{x}_j$ using gradient boosting with validation-based calibration. Our six methods address different challenges in job duration prediction:

(1) Conformal Quantile Regression (CQR) (Romano et al., 2019) addresses prediction uncertainty by learning the conditional distribution rather than just point estimates. We train three LightGBM models with quantile loss at $\alpha \in \{0.1, 0.5, 0.9\}$ to predict the 10th, 50th, and 90th percentiles of job duration. On the validation set, we compute the conformal width $w = \text{quantile}_{0.6}(|Q_{0.1} - y|, |y - Q_{0.9}|)$ from residuals, which captures the typical prediction error. The final prediction blends the median $Q_{0.5}$ with the calibrated interval bounds $[Q_{0.5} - w, Q_{0.5} + w]$ using Ridge regression, along with contextual features like group means. This approach is particularly effective for jobs with high uncertainty—for instance, experimental ML training jobs where duration depends on convergence criteria, or data processing jobs where input size varies significantly. The method provides both accurate point estimates and reliable confidence intervals.

(2) Isotonic Calibration (Zadrozny & Elkan, 2002; Kuleshov et al., 2018) corrects systematic prediction biases while preserving ranking order. The method fits a monotonic non-decreasing function $\phi : \mathbb{R} \to \mathbb{R}$ mapping raw predictions to calibrated values, ensuring $\phi(x_1) \leq \phi(x_2)$ whenever $x_1 \leq x_2$. This is crucial when the model consistently over-predicts short jobs (e.g., quick validation scripts that always take 5 seconds but are predicted as 30 seconds) or under-predicts long jobs (e.g., full model training that takes 10 hours but is predicted as 2 hours). The isotonic regression finds the optimal step function that minimizes squared error on the validation set while maintaining mono-

tonicity. This property is essential for scheduling decisions where relative job ordering matters—if job A is predicted to be shorter than job B, this relationship is preserved after calibration.

(3) Meta-Stacking (Wolpert, 1992) leverages model diversity to improve robustness. We train four base models with different loss functions: (i) L2 loss for standard regression, (ii) Huber loss ($\delta = 0.9$) for robustness to outliers like crashed jobs or anomalously long runs, (iii) quantile loss for median prediction, and (iv) heavily regularized L2 ($\alpha = 0.5, \lambda = 1.0$) to prevent overfitting. Each model captures different aspects: L2 minimizes average error, Huber handles extreme cases, quantile focuses on the median behavior, and regularized models provide stable baselines. The meta-learner (another LGBM) takes these base predictions, their standard deviation (measuring disagreement), and contextual features (group history, signature statistics) as input. It learns non-linear combinations—for example, trusting the Huber model more when base predictions diverge significantly (indicating potential outliers), or weighting the regularized model higher for users with limited history.

(4) Two-Stage Gated Experts (Jordan & Jacobs, 1994) recognizes that different job types require different prediction strategies. The gating network (classifier) first categorizes jobs into three types based on the 30th and 70th percentiles of training durations: (i) *short jobs* (>30th percentile, typically <100s): quick validation runs, status checks, or small data samples; (ii) *medium jobs* (30th–70th percentile, 100s–1000s): regular training epochs, moderate data processing; (iii) *long jobs* (>70th percentile, >1000s): full model training, large-scale data processing, or hyperparameter sweeps. Each category gets a specialized expert model with appropriate complexity—simple models for predictable short jobs, complex deep trees for variable long jobs. The final prediction aggregates expert outputs weighted by soft probabilities: $\hat{y} = \sum_{c \in \{\text{short, med, long}\}} P(c|\mathbf{x}) \cdot E_c(\mathbf{x})$. This prevents short jobs from being influenced by patterns from marathon training runs and vice versa.

(5) Weighted Recency (Gama et al., 2014) adapts to temporal drift in workload patterns. Computing clusters exhibit temporal patterns: new framework releases change typical training times, approaching deadlines increase job submissions, and hardware upgrades affect processing speeds. We train three models on progressively recent data windows: (i) full history for stable long-term patterns, (ii) recent 50% for medium-term trends, (iii) recent 20% for immediate patterns. Each training sample receives weight $w_t = \exp(-\lambda(T - t))$ where T is the current time and λ controls decay rate. Models are combined using validation performance weights—if recent models show lower validation error, they receive higher weight in the ensemble, automatically adapting to drift. For example, after a PyTorch version upgrade that speeds up training by 30%, the recent-20% model would quickly adapt while the full-history model provides stability.

(6) Historical Recency-Aware with Shrinkage (HRAS) addresses the cold-start problem for rare job signatures. A signature combines user, group, workload type, and resource requirements (bucketed into deciles). Rare signatures include: (i) new users or groups with no history, (ii) unusual resource combinations (e.g., user `alice` from `vision_group` suddenly requesting 8 GPUs when historically using only CPUs), (iii) infrequent workload types (e.g., monthly financial reports in a primarily ML-focused cluster). For signature s with n_s historical observations and mean duration μ_s, we apply Empirical Bayes shrinkage: $\bar{\mu}_s = (n_s\mu_s + \lambda\mu_0)/(n_s + \lambda)$, where μ_0 is the global mean and $\lambda = 5$ is the shrinkage strength. When $n_s = 0$ (completely new pattern), the prediction equals the global mean. As n_s grows, the prediction gradually shifts toward the signature-specific mean. The exponentially weighted component gives more weight to recent instances of the signature, capturing evolution in user behavior.